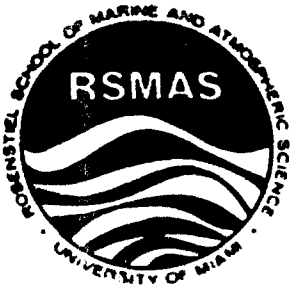

RSMAS TECHNICAL REPORT 94-001

MEASUREMENTS OF COASTAL CURRENTS USING A SHIP BASED VHF RADAR SYSTEM

by

Richard A. Skop, Duncan B. Ross, Nicholas J. Peters and Lila Chamberlain

Division of Applied Marine Physics
Rosenstiel School of Marine and Atmospheric Science
University of Miami
Miami, FL 33149

March 1994

Prepared for the Naval Research Laboratory (SSC)
and the Office of Naval Research
under grant N00014-93-1-G900

Contents

Introduction

Radio wavelength (VHF/HF) Doppler radar techniques have been successfully used to observe coastal currents from shore based sites for many years (cf. Barrick, 1972; Stewart and Joy, 1974; Schott et al., 1986; Prandle, 1987; Shay et al., 1992; Chemi et al., 1993). The radar technique exploits the Bragg resonant backscatter phenomenon of electromagnetic waves by ocean waves exactly one-half the wavelength of the emitted radiation whose crests are oriented perpendiculary to the axis of the radar beam. Range-gated Doppler processing of the received signal is then used to observe the wave phase velocity toward or away from the radar. Any shift in the observed wave velocity from its theoretical deep-water value is related directly to the vector component of the current moving toward or away from the radar site. Use of two systems to determine radial currents at a given coordinate from two directions allows calculation of the resultant current speed and direction. A mapping capability is obtained by means of scanning with a phased array antenna.

The University of Miami Ocean Surface Current Radar (OSCR) is a pulsed radar which utilizes a Yagi transmit antenna and a line array receive antenna. In its VHF (50 MHz) mode of operation, the system has a range of 12 km and a resolution of 250 m. The Bragg resonant wavelength is 3 m.

In December 1993, one of two OSCR VHF sites was configured aboard the 50 m research vessel COLUMBUS ISELIN, anchored in a four-point mooring 5 km from the second site on Key Biscayne, FL. A six channel accelerometer system was used to obtain ship motion measurements. The purpose of this experiment was an initial evaluation of using an OSCR type system to map nearshore coastal currents from a ship. Such capability would be useful in many coastal survey operations.

Specifically, the experiment was designed to address two questions. The first question concerned the influence of ship superstructure (multi-path propagation) on the received Doppler spectra. To examine this question, the receive antenna array was mounted in two configurations: one being the normal "up" position and the other being a "down" position in which the ship hull acted as a predictable reflecting plane. Our results indicate little superstructure effect on the received spectra.

The second question concerned the influence of ship motions (ship-induced Doppler) on the received Doppler spectra. Such influences can be predicted and, for periodic ship motions, lead to periodic frequency modulations about the Doppler frequency. These frequency modulations lead, in turn, to a series of extraneous spectral peaks that are symmetric about the "true" peak and that have a magnitude dependent on the modulation index m (Oppenheim et al., 1983). Here, $m = vT/(2\pi\lambda)$ where T is the period of the ship motion, V is a characteristic velocity associated with this motion and λ is the Bragg resonant wavelength. Because of the four-point mooring and the light sea conditions encountered during our experiment, the measured values of m were such that ship motions would be expected to have had negligible effect on the received Doppler spectra. The received spectra confirm this expectation.

FIGURE 1. VHF OSCR site on Key Biscayne, FL.

Vector current maps constructed from the radial current data obtained by the ship based and land based systems are low in noise and show the circulation to be tidally dominated. The validity of these maps is demonstrated by comparisons with drifter measurements and with known tidal flows off Key Biscayne.

Overall, our experiment demonstrates the practicality of mapping nearshore currents from a ship using an OSCR type system.

Experimental Setup

One of the two VHF OSCR sites was on Key Biscayne, FL. This site is shown in Figure 1. The site was configured with a 16 element, half-wavelength (i.e., 3 m) spacing, linear receive array. The weighting factors for the 16 elements are given in Table 1. With this weighting, the beamwidth of the array at the 3 dB down point of the main lobe was 6.8° for ground plane reception.

TABLE 1. Weighting Factors for the 16 Element, Shore Based OSCR Receive Array (Counting from Outside Element)

Element Number	Weighting Factor
1	1.0992
2	1.2071
3	1.3065
4	1.3945
5	1.4683
6	1.5258
7	1.5652
8	1.5852
9	1.5852
10	1.5652
11	1.5258
12	1.4683
13	1.3945
14	1.3065
15	1.2071
16	1.0992

The second OSCR site was aboard the 50 m research vessel COLUMBUS ISELIN. The vessel was anchored in a four-point mooring approximately 5 km off Key Biscayne. Throughout the measurement period, the winds were relatively steady at 8 to 12 kt and were predominantly from a Northeasterly to Easterly direction as shown in Figure 2. The sea-state was estimated at between 1.0 and 1.5. Under these conditions, the ship maintained a heading of 177.3° with a standard deviation of 1.3°. The record of the ship's heading is plotted in Figure 3.

The site aboard the COLUMBUS ISELIN is shown in Figure 4. The Yagi transmit antenna was located near the bow of the vessel and the site was configured with a 12 element, half-wavelength spacing, linear receive array. The receive elements were mounted on sections of C-channel that were positioned slightly outboard of the hull. The individual elements could be mounted to the channels in a normal "up" configuration as shown in Figure 4 or inverted into a "down" configuration. In the latter configuration, the hull functioned as a reflecting plane for the receive array. The weighting factors and hull offsets for the 12 elements are given in Table 2. The calculated beam patterns for ground plane reception for the "up" and "down" 12 element receive array configurations are shown in Figures 5a and 5b, respectively. The "up" configuration calculations were made assuming no superstructure effects and give a beamwidth of 8.8° at the 3 dB down point of the main lobe. The "down" configuration calculations were made using the hull offsets from Table 2. We see that the "up" and "down" configuration beam patterns are essentially identical because the hull offsets in the "down" configuration are small relative to the carrier wavelength of 6 m.

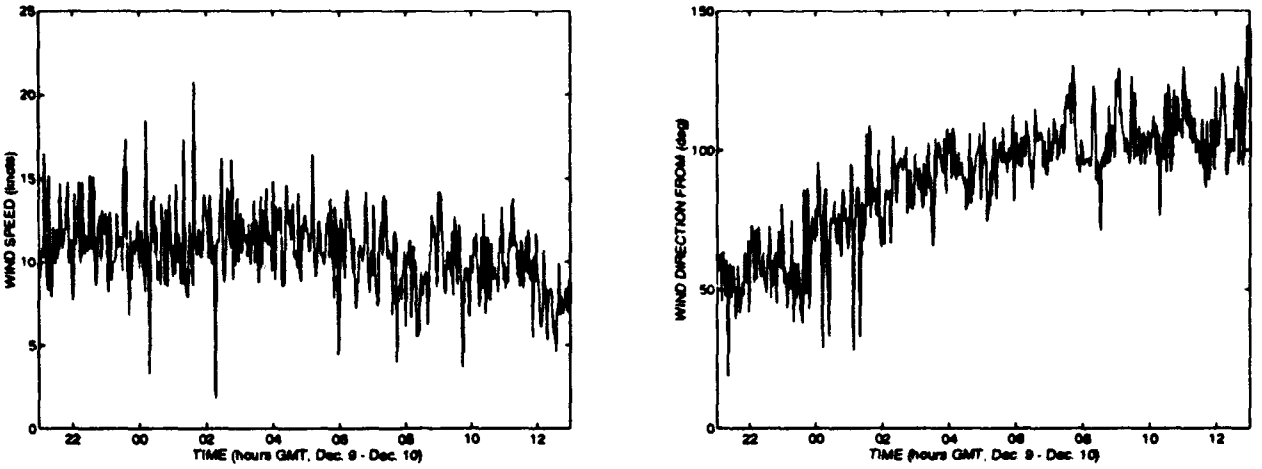

FIGURE 2. Wind speed and direction during OSCR shipboard experiment.

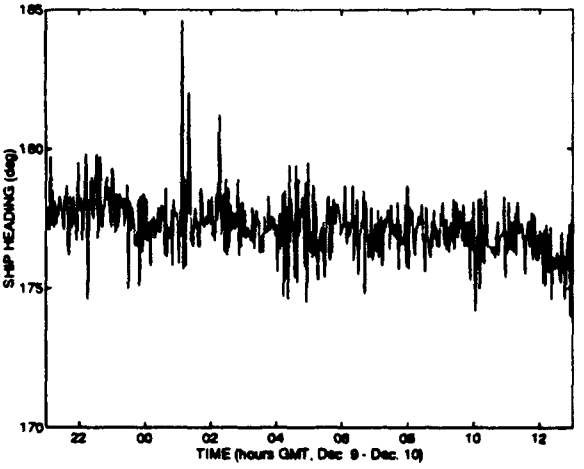

FIGURE 3. Ship heading during OSCR shipboard experiment.

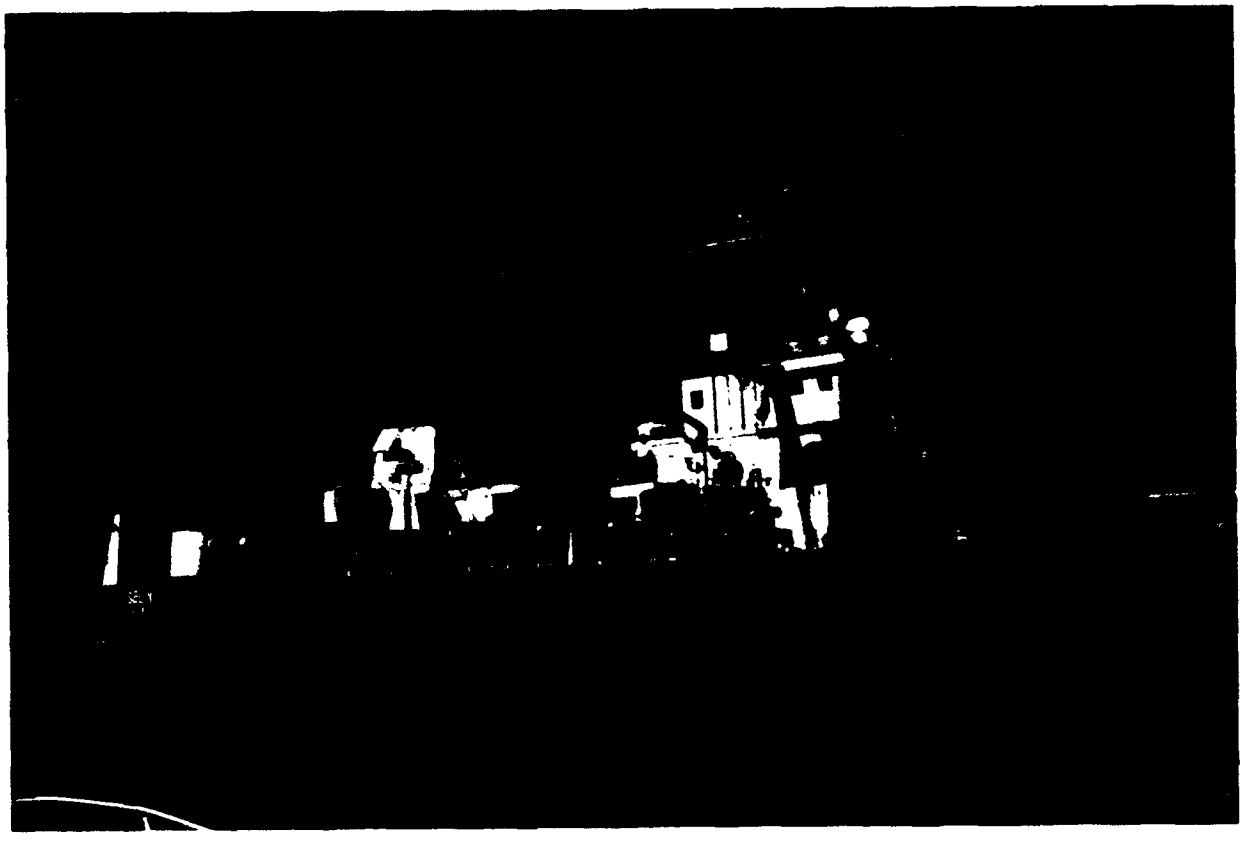

FIGURE 4a. The OSCR site aboard the 50 m research vessel COLUMBUS ISELIN. The receive array elements located toward the aft of the vessel are visible.

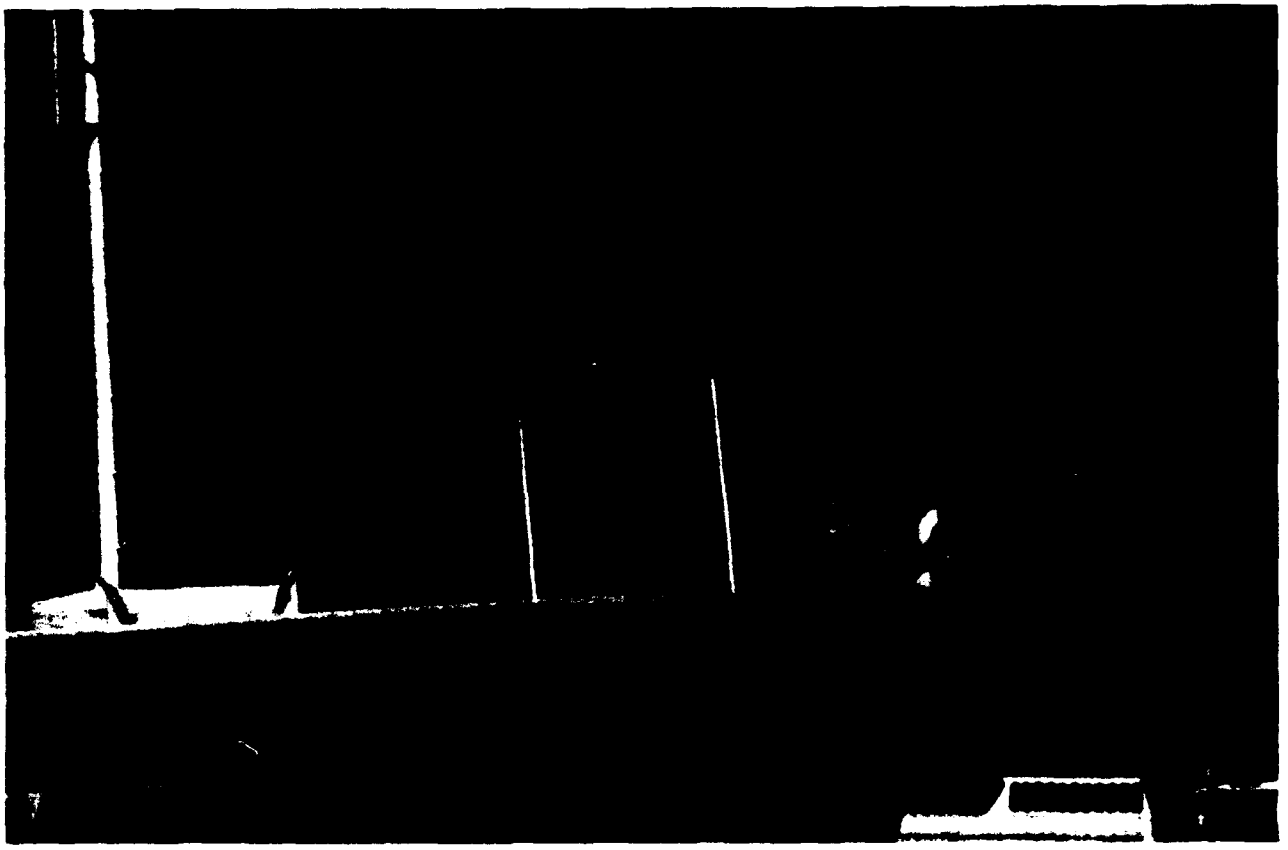

FIGURE 4b. The Yagi VHF transmit antenna mounted in the bow of the COLUMBUS ISELIN.

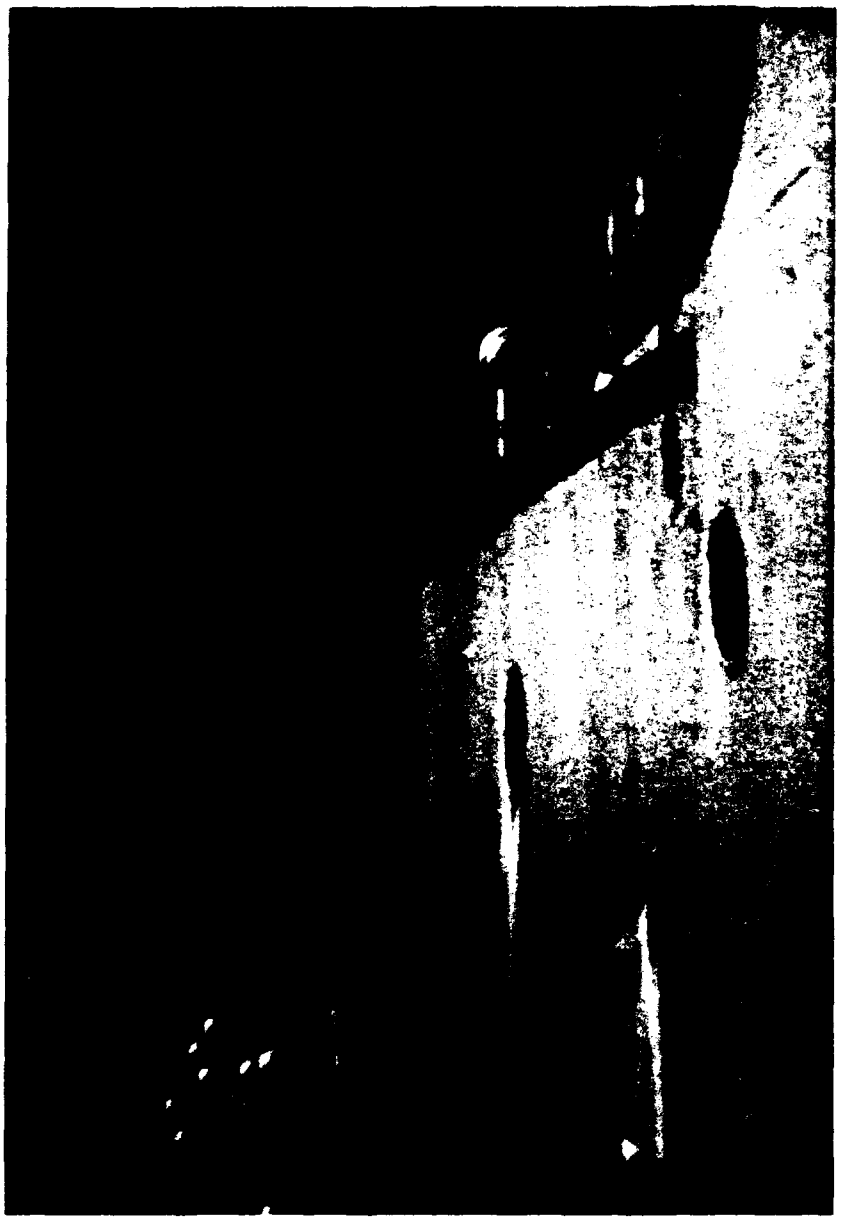

FIGURE 4c. The 12 element receive array mounted along the starboard side of the COLUMBUS ISELIN.

TABLE 2. Weighting Factors and Hull Offsets for the 12 Element, Ship Based OSCR Receive Array (Counting from Aft Element)

Element Number	Weighting Factor	Hull Offset (m)
1	1.3065	0.5080
2	1.3945	0.4572
3	1.4683	0.4064
4	1.5258	0.3556
5	1.5652	0.3048
6	1.5852	0.2540
7	1.5852	0.2032
8	1.5652	0.1524
9	1.5258	0.1524
10	1.4683	0.2540
11	1.3945	0.3048
12	1.3065	0.3556

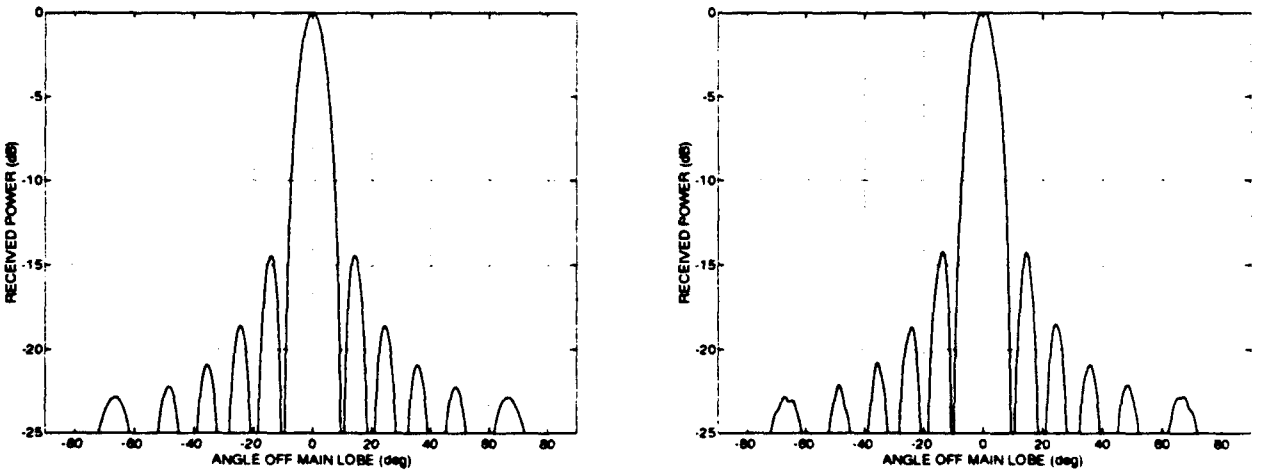

(a) (b)

FIGURE 5. Ground plane beam patterns for 12 element receive array aboard the COLUMBUS ISELIN: (a) "up" configuration, (b) "down" configuration.

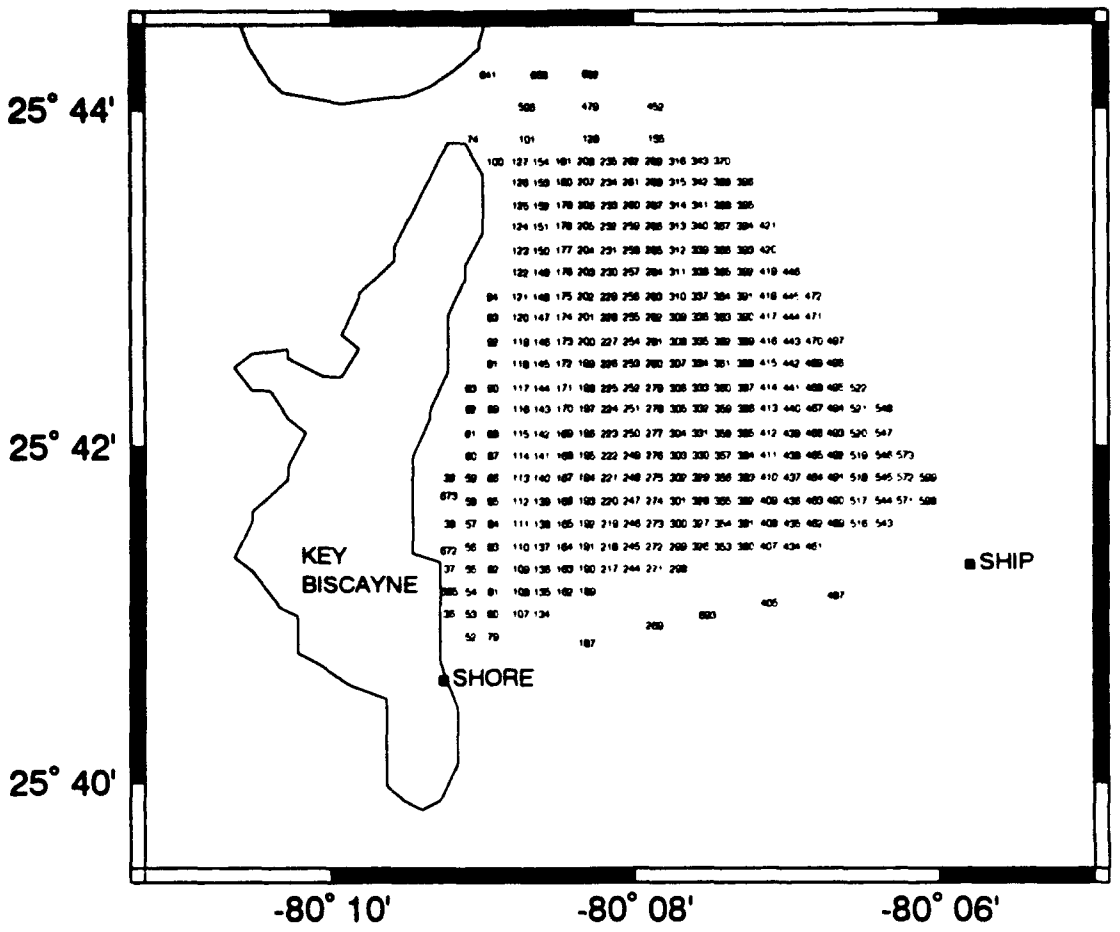

FIGURE 6. Locations of ship and shore based OSCR sites for the shipboard experiment. Also shown is the footprint (i.e., cell positions and cell numbers) of the OSCR coverage.

The locations of the two OSCR sites are shown in Figure 6. Also shown in Figure 6 are the OSCR cell positions and corresponding cell numbers at which radial currents were measured during the experiment. One set of cells lies along the line-of-sight between the ship and shore based sites. The other set of cells is in the region where vector currents were constructed from the measured radial currents.

A six channel, piezoresistive accelerometer system was installed on the COLUMBUS ISELIN to obtain ship motions. Three of the accelerometers were mounted on a triaxial block which was attached to one of the C-channels and aligned parallel to the ship fixed x, y and z axes. Two of the other accelerometers were mounted on a biaxial block which was aligned parallel to the ship fixed x and z axes. The biaxial block was located 5.27 m directly inboard of the triaxial block. The final accelerometer was mounted on a uniaxial block which was aligned parallel to the ship fixed z axis and located 3.20 m directly aft of the triaxial block.

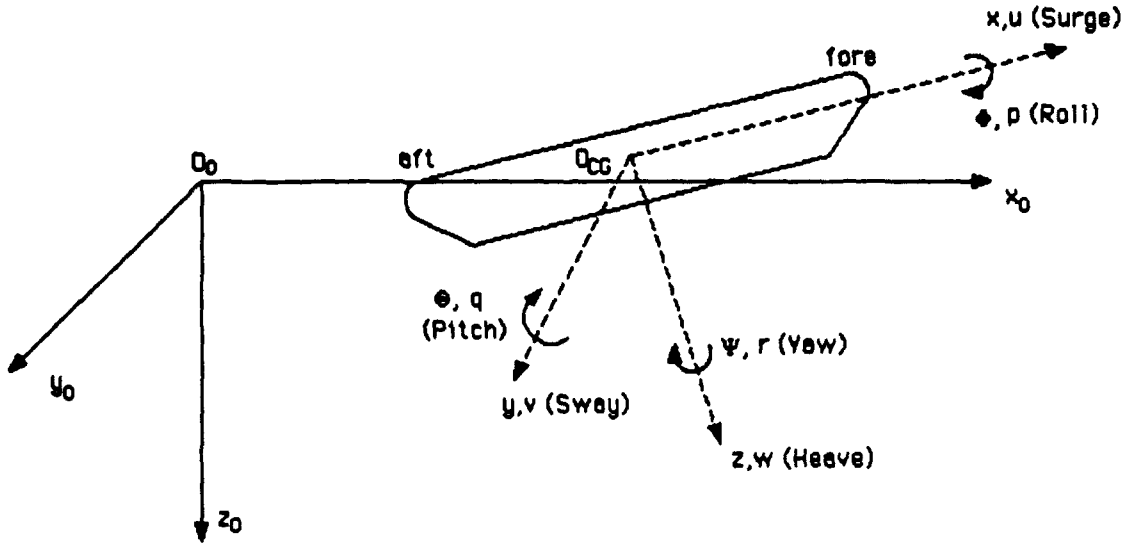

FIGURE 7. Ship fixed coordinate system.

The ship fixed coordinate system is sketched in Figure 7. Its origin is taken as the center of gravity of the vessel with the x axis increasing to fore, the y axis increasing to starboard and the z axis increasing to keel. The local linear velocity vector $\vec{U}_i$ at any point i on the ship is given by

$$\vec{U}_i = u_i\hat{i} + v_i\hat{j} + w_i\hat{k} \tag{1}$$

where $\hat{i}$, $\hat{j}$ and $\hat{k}$ are the unit vectors and u_i, v_i and w_i are the local velocity components along the ship fixed x, y and z axes, respectively. The ship angular velocity vector $\vec{\Omega}$ is given by

$$\vec{\Omega} = p\hat{i} + q\hat{j} + r\hat{k} \tag{2}$$

Here, p is the roll rate about the x axis, q is the pitch rate about the y axis and r is the yaw rate about the z axis. $\vec{\Omega}$ and $\vec{U}_i$ can be determined from the accelerometer data. Letting the subscripts t, b and u denote the triaxial, biaxial and uniaxial accelerometer blocks, respectively, we have

$$p = \frac{w_t - w_b}{5.27}, \qquad q = \frac{w_u - w_t}{3.20}, \qquad r = \frac{u_b - u_t}{5.27} \tag{3}$$

and

$$\vec{U}_i = \vec{U}_t + \vec{\Omega} \times \vec{R}_{ti} \tag{4}$$

In the latter equation, $\vec{R}_{ti}$ is the position vector from the triaxial block to the point i.

Ship Motion Effects

In the presence of ship motions, the modulation frequency f_d perceived at the ith element of the OSCR receive array is

$$f_d = \pm\left(\frac{g}{2\pi\lambda}\right)^{1/2} + \frac{u_r(R,\theta)}{\lambda} + \frac{\cos\theta}{2\lambda t}\int_0^t (v_{tr} + v_i)\, d\tau \tag{5}$$

Here, g is the gravitational acceleration and the first term on the right-hand-side of the equation corresponds to the frequency of the Bragg resonant wave (plus for a wave propagating towards the receive array, minus for a wave propagating away). The second term on the right-hand-side gives the shift in the modulation frequency due to the radial component u_r of the surface current at range R from the receive array and at angle θ to the boresight of the array. The radial component of the surface current is taken as positive advancing towards the array. The final term on the right-hand-side of equation (5) gives the shift in the modulation frequency due to ship motions. In this term, t is time and v_{tr} and v_i are, respectively, the velocities of the transmit antenna and the ith element of the receive array along the ship fixed y axis. In obtaining the final term of equation (5), use has been made of the fact that both the boresight of the transmit antenna and the boresight of the receive array were along the ship fixed y axis. For the periodic ship motions expected in the anchored configuration, $v_{tr} + v_i$ can be expressed as

$$v_{tr} + v_i = 2V\cos\frac{2\pi t}{T} \tag{6}$$

where $V = (V_{tr} + V_i)/2$ with V_{tr} and V_i being the magnitudes of v_{tr} and v_i, respectively, and where T is a characteristic period of the ship motion. Substituting equation (6) into equation (5), the modulation frequency is found as

$$f_d = \pm\left(\frac{g}{2\pi\lambda}\right)^{1/2} + \frac{u_r(R,\theta)}{\lambda} + \frac{VT\cos\theta}{2\pi\lambda t}\sin\frac{2\pi t}{T} \tag{7}$$

The modulation function $\psi(t)$ perceived at the ith element of the OSCR receive array is composed of terms containing either $\cos(2\pi f_d t)$ or $\sin(2\pi f_d t)$. To examine the effects of periodic ship motions on the modulation function, it suffices to consider only one of these terms. Also, without loss of generality, it suffices to set u_r and θ equal to zero in equation (7). Hence, with λ = 3 m as appropriate to the VHF mode of OSCR operation, the modulation function becomes

$$\psi(t) = \cos\left[2\pi\left(0.7214\,t + \frac{VT}{6\pi}\sin\frac{2\pi t}{T}\right)\right] \tag{8}$$

From this equation, we see that the influence of periodic ship motions is to introduce periodic frequency modulations about the Doppler frequency into the modulation function. As discussed by Oppenheim et al. (1983), these frequency modulations lead to a series of extraneous spectral peaks that are symmetric about the "true" spectral peak and that have a magnitude dependent on $VT/(6\pi)$. This behavior is demonstrated in Figures 8a through 8c where the power spectra of $\psi(t)$ are shown for increasing values of V at a ship period fixed at $T = 20$ s. To be consistent with the operation of the OSCR system, the power spectra are based on 512 samples of equation (8) at a sampling interval of 0.32768 s. Further, the spectra are normalized by the square of the length of the sampling period, i. e. by $(0.32768 \times 511)^2$.

In each of Figures 8a through 8c, the dB difference between the value of the power spectrum at the expected spectral peak and the value of the power spectrum at the maximum sideband peak is tabulated. This dB difference is also plotted in Figure 9 as a function of VT for various values of T. We see from Figure 9 that the dB difference is sensitive to the value of VT but relatively insensitive to the value of T. In selecting possible spectral pairs, the OSCR software for the most part ignores any peaks more than 6 dB down from the dominant peak. From Figure 9, we would then anticipate that ship motions would have negligible effects on the received Doppler spectra for values of VT less than 2.75 m.

For the OSCR configuration aboard the COLUMBUS ISELIN, the motions of each of the receive elements were smaller than or tended to cancel out the motions of the transmit antenna. Hence, the "worst-case" effects of ship motions can be found by setting $v_i = v_{tx}$ in equation (6); that is, by setting $V = V_{tx}$. Typical zero-meaned velocity records at the transmit antenna, as determined from the accelerometer measurements and equations (2) through (4) with $\vec{R}_{ti}$ = {32.5 m, -5.5 m, -5.5 m}, are shown in Figures 10a, 10b and 10c. The times at which the records were taken coincide with three different, five minute send/receive cycles of the OSCR system. We note from Figure 10 that the magnitudes of the recorded velocities at the transmit antenna were generally less than 1.5 m/s indicating the mild sea conditions encountered during the experiment.

The normalized Fourier transform $\tilde{V}(f)$ of v_{tx} is defined by

$$\tilde{V}(f) = \frac{1}{T_R}\int_0^{T_R} v_{tx} e^{-j2\pi ft} dt \tag{9}$$

where T_R is the record length of v_{tx}. There is a direct equivalence between the magnitude V of the velocity at a given frequency and $|\tilde{V}(f)|$ (Brigham, 1974). Hence, at a given frequency, we also have

$$VT = \frac{|\dot{V}(f)|}{f} \tag{10}$$

In Figures 11a, 11b and 11c, the values of VT corresponding, respectively, to the velocity records at the transmit antenna shown in Figures 10a, 10b and 10c are plotted. We observe from Figure 11 that the peak values of VT are on the order of 1.0 m. Transposing this value of VT to Figure 9, we find that the sideband Doppler peaks due to ship motions during our experiment would be expected to be at least 15 dB down from the true Doppler peaks.

Doppler spectra measured at cell 693 from both the ship and shore based OSCR sites are shown in Figures 12a through 12c. The times of the spectral measurements are coincident with the times of the ship motion measurements shown in Figure 10. Cell 693, as indicated in Figure 6, was along the line-of-sight between the two OSCR installations. In consequence, the spectra obtained by the ship and shore sites at cell 693 should be mirror images of each other in the absence of ship motions and noting that a constant dB shift along the vertical axis of one of the spectra is consistent with differences in received power at the two sites. The mirror images of the shore based spectra overlayed on the ship based spectra are shown in Figures 13a through 13c. It is apparent from Figure 13 that the mirrored spectra are very similar, even down to secondary and tertiary peaks. Hence, our expectation that the ship motions measured during the experiment would have negligible effects on the received Doppler spectra is verified by the line-of-sight spectral data.

Ship Superstructure Effects

The ship based Doppler spectra shown in Figures 12a, 12b and 12c were obtained with the receive array in its "up", "down" and "up" configurations, respectively. With the receive array in its "down" configuration, the ship hull functioned as a predictable reflecting plane for the array. The ground plane beam pattern of the array in its "down" configuration (Figure 5b) is not substantially different than the beam pattern of the 16 element, shore based receive array. With similar beam patterns, Doppler spectra measured using the "down" configuration of the receive array and Doppler spectra measured from the shore based site should be, in the absence of ship motions, mirror images for line-of-sight cells. We have already observed this mirror image property in Figure 13b. However, we have also observed this mirror image property in Figures 13a and 13c which correspond to the "up" configuration of the receive array. Hence, at least for the receive array setups used during our experiment, there were no discernable ship superstructure effects on the received Doppler spectra.

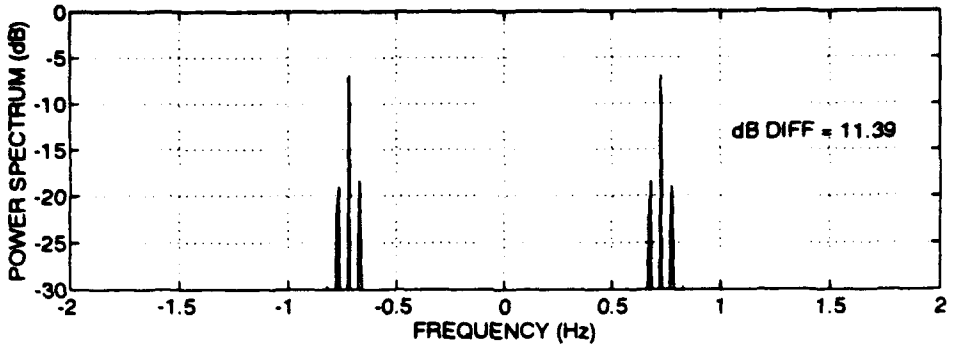

(a)

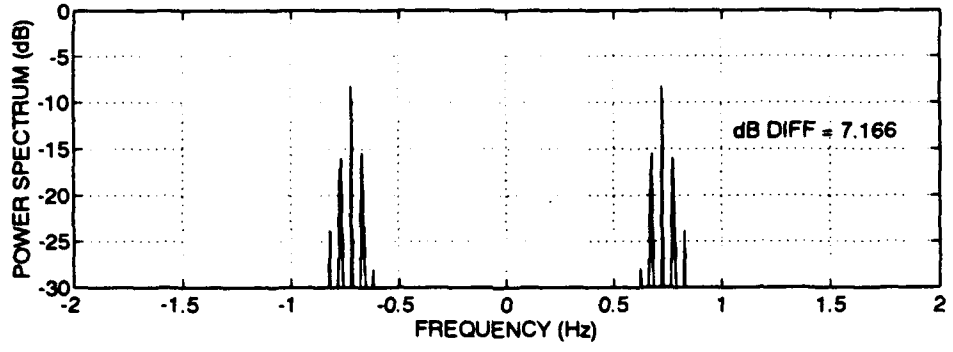

(b)

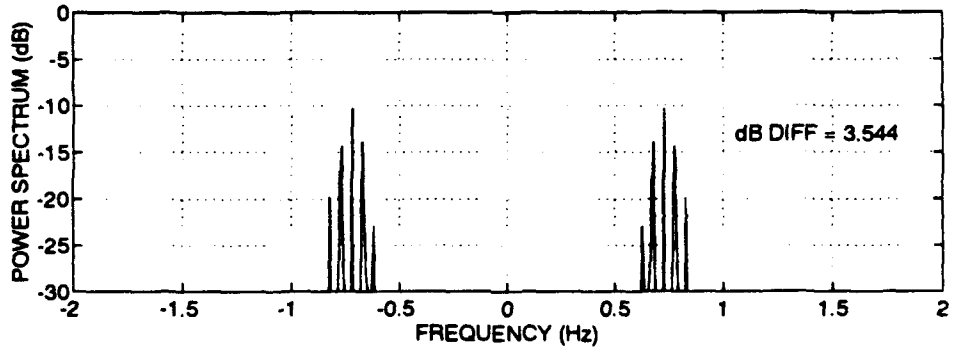

(c)

FIGURE 8. Power spectra of modulation function defined in equation (8) for a ship period T = 20 s: (a) VT = 0.10 m, (b) VT = 0.15 m, (c) VT = 0.20 m.

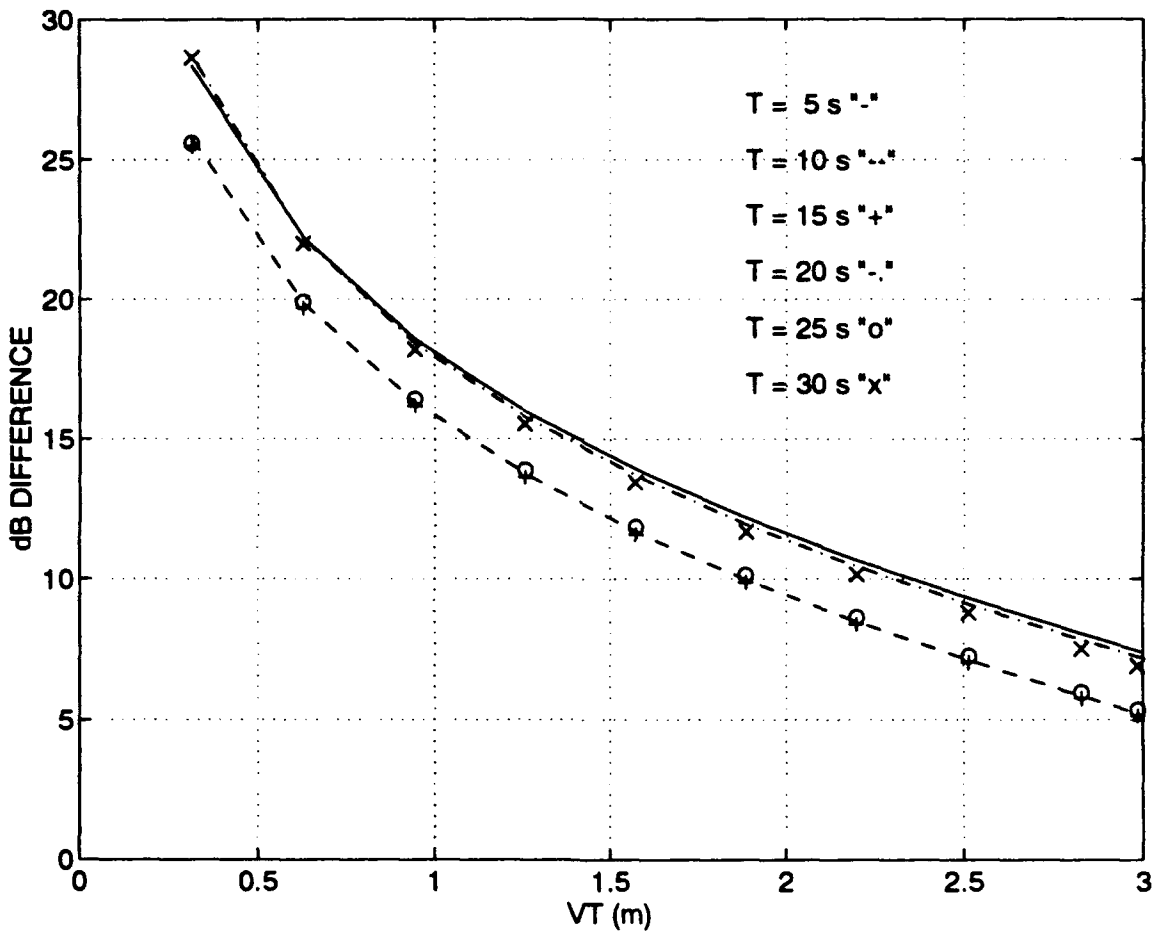

FIGURE 9. dB difference between spectral value at expected spectral peak and spectral value at maximum sideband peak.

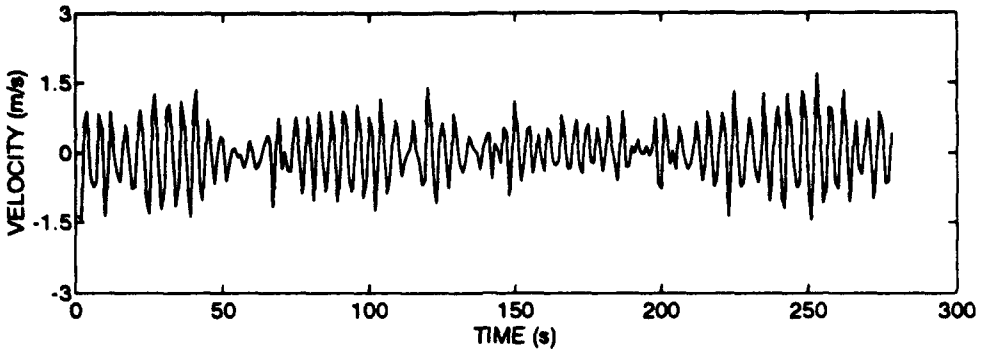

(a)

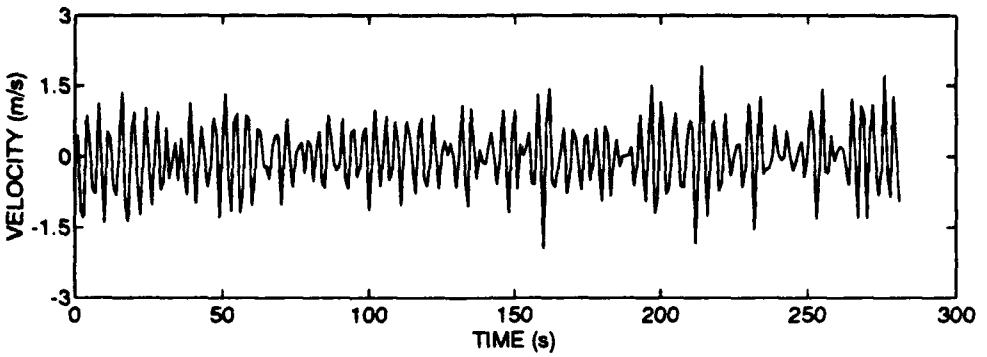

(b)

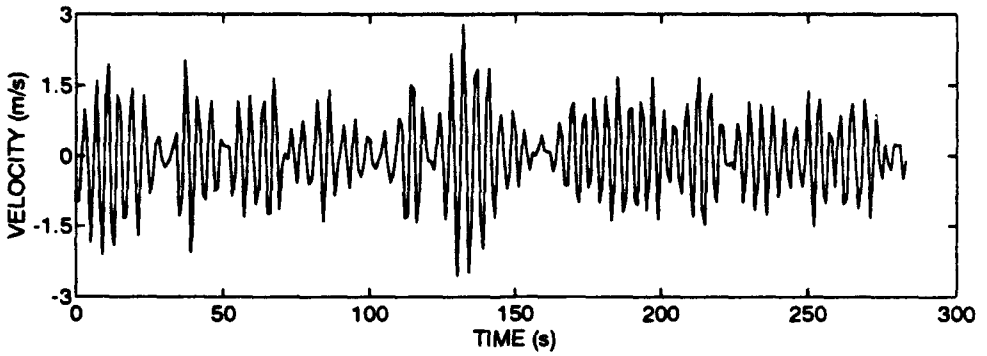

(c)

FIGURE 10. Velocity records at transmit antenna during shipboard transmit cycles. (a) 2220 GMT on Dec. 9, (b) 0040 GMT on Dec. 10, (c) 1200 GMT on Dec. 10.

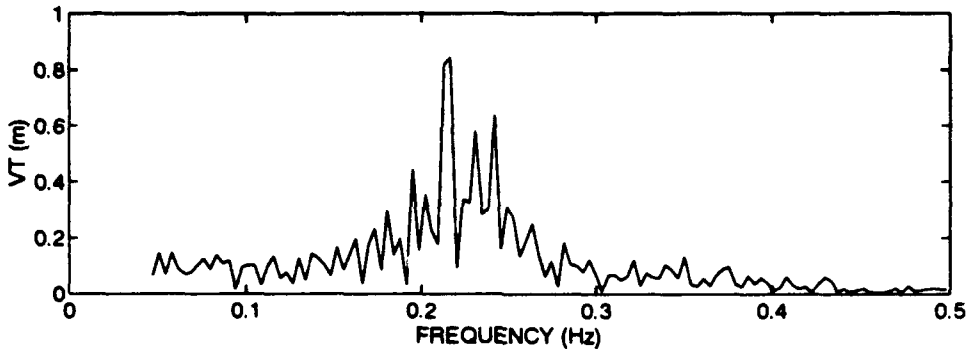

(a)

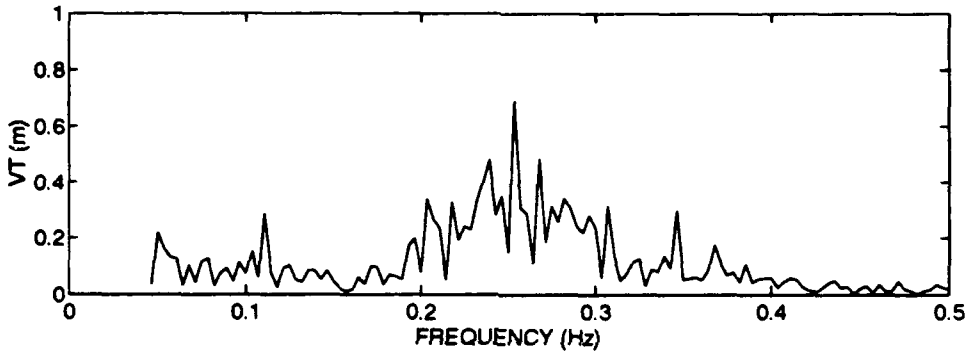

(b)

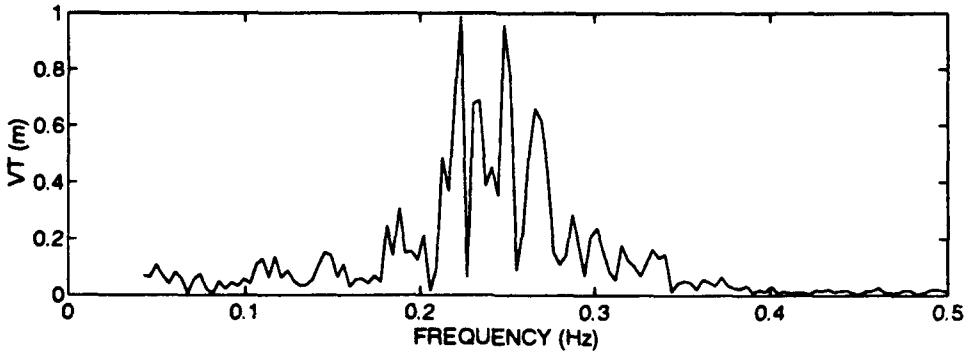

(c)

FIGURE 11. Values of $VT = |\tilde{V}(f)|/f$ corresponding to the velocity records in Figure 10. (a) 2220 GMT on Dec. 9, (b) 0040 GMT on Dec. 10, (c) 1200 GMT on Dec. 10.

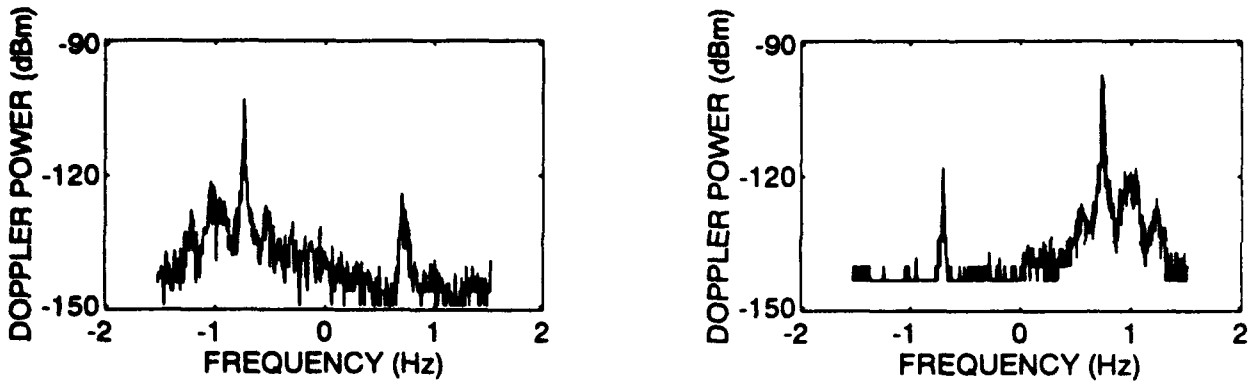

(a)

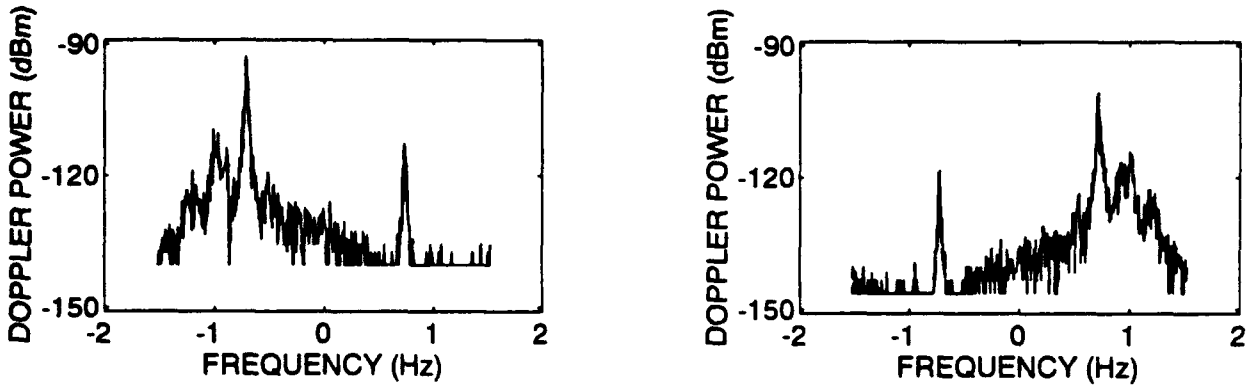

(b)

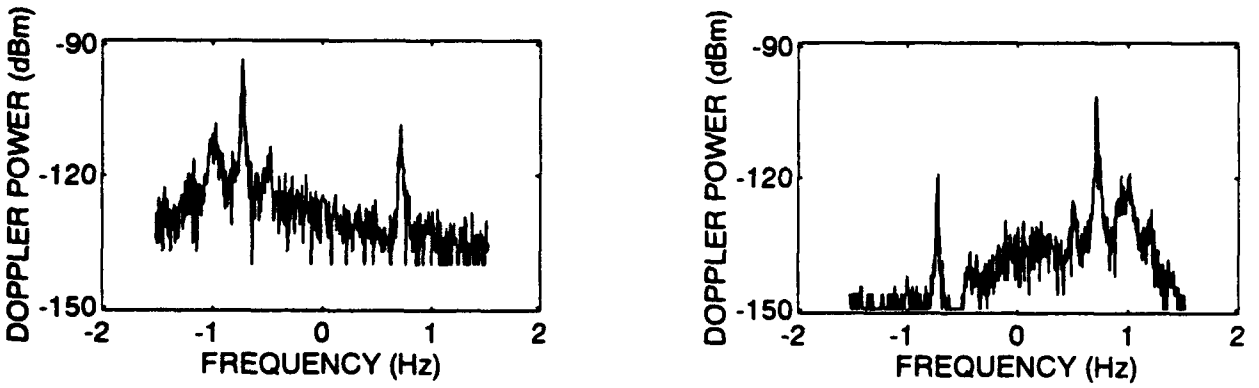

(c)

FIGURE 12. Doppler spectra at cell 693 located along the line-of-sight between the ship and shore based OSCR sites. The ship based spectra are on the left; the shore based spectra are on the right. (a) 2220 GMT on Dec. 9, (b) 0040 GMT on Dec. 10, (c) 1200 GMT on Dec. 10.

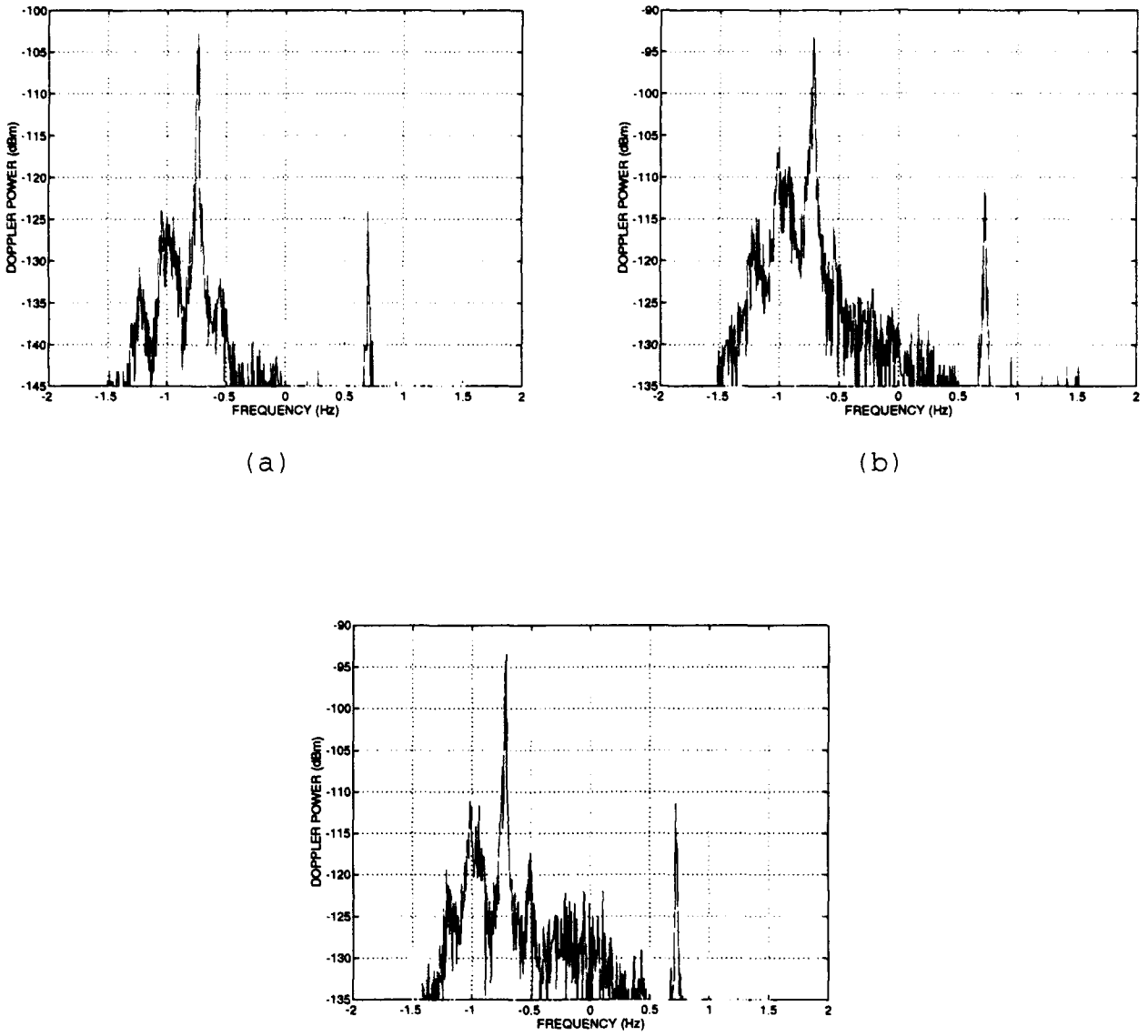

FIGURE 13. Mirror images of the shore based spectra (red) overlayed on the ship based spectra (yellow). (a) 2220 GMT on Dec. 9, (b) 0040 GMT on Dec. 10, (c) 1200 GMT on Dec. 10.

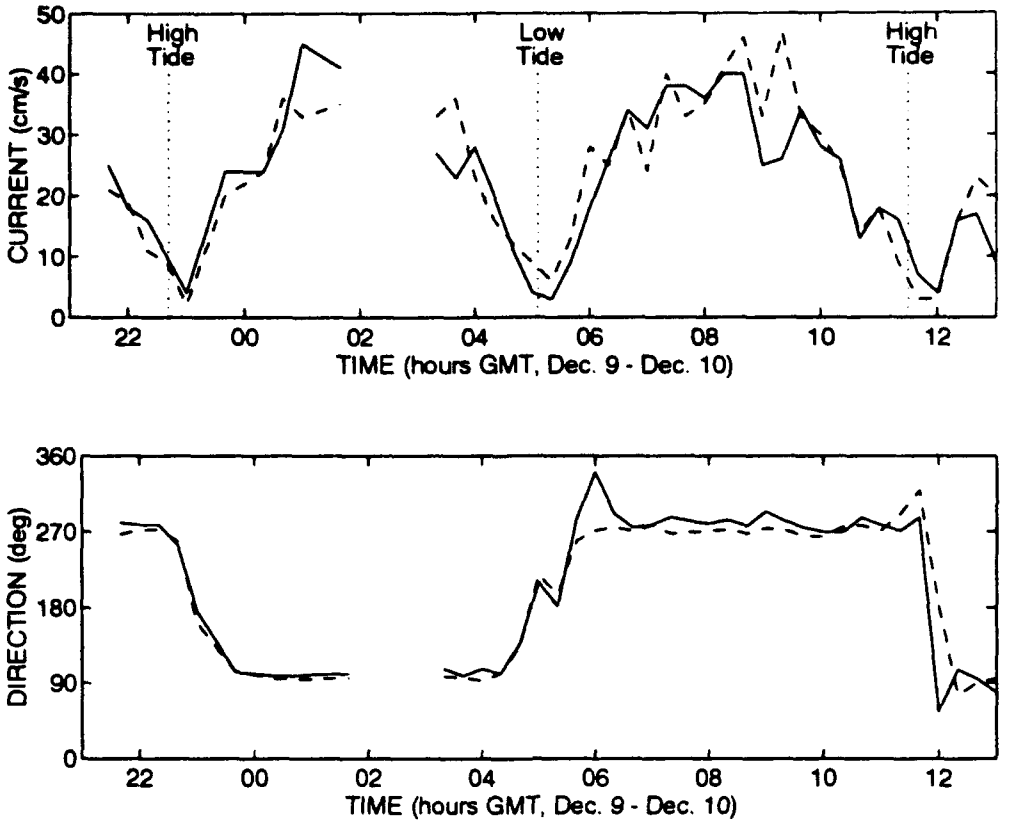

FIGURE 14. Surface current magnitudes and directions observed at cells 101 (solid lines) and 506 (dashed lines). The cells were adjacent to each other and located at the mouth of a tidal inlet between the ocean and Biscayne Bay. The times indicated for the high and low tides were obtained from tide tables.

Surface Current Observations

The magnitudes and directions of the surface currents observed by the OSCR system at cells 101 and 506 during the course of the experiment are summarized in Figure 14. These two cells, as shown in Figure 6, were located just north of Key Biscayne at the mouth of an east-west inlet between the Atlantic Ocean and Biscayne Bay. The inlet, known as Bear Cut, is characterized by strong tidal flows which reverse rapidly around the high and low ebbs. From Figure 14, we see that, between 0000 GMT and 0400 GMT on Dec. 10, the OSCR system observed an outgoing tide with a direction of 90° and a magnitude of 30 to 40 cm/s. Between 0600 GMT and 1000 GMT on the same day, the system observed an incoming tide with a direction of 270° and a magnitude of 30 to 40 cm/s. Also indicated on Figure 14, are the times of the high and low tides at the mouth of Bear Cut as determined from tide tables. The concurrence between the ebbs observed by the OSCR system and the high and low tides obtained from the tide tables is evident.

Four surface current maps generated by the OSCR system during the experiment are pictured in Figure 15. The upper left map shows the incoming tide at 2200 GMT on Dec. 9, the upper right map shows the subsequent high tide near 2300 GMT on Dec. 9, the lower left map illustrates the outgoing tide at 0200 GMT on Dec. 10, and the lower right map illustrates the subsequent low tide near 0500 GMT on Dec. 10. The details of the surface currents obtainable with the OSCR system are apparent. Especially iinteresting in Figure 15 is the jetlike behavior of the tides near the northern tip of Key Biscayne. That is, the incoming tide diverges into northerly and sourtherly flows near the northern tip. Similarly, the outgoing tide converges near the northern tip.

To corroborate the surface currents measured by the OSCR system, two types of drifters were deployed during the experiment. The AMP drifters were syntactic foam disks, 9.0 cm in diameter and 3.5 cm in thickness, which were weighted to float with the top edge just at the water surface. The CODE drifter consisted of four vertical panels arranged in a crossed configuration. The panels extended from the water surface to a 1.0 m depth. The deployment and recovery times of the drifters, together with the corresponding geographical coordinates, are summarized in Table 3. From Table 3, we note that the drifters were deployed approximately three hours before and recovered approximately two hours before the first OSCR measurements at 2200 GMT on Dec. 9. However, the period over which the drifters were tracked coincided to an incoming tide during which, as we have seen in Figure 14, the currents are relatively steady. Similary, the OSCR measurements at 2200 GMT coincided to the last stages of this steady incoming tide. Hence, comparisons between the drifter and OSCR measurements of the prevailing surface currents can be expected to contain some degree of validity.

In Table 4, the mean currents and mean current directions observed by the AMP and the CODE drifters are tabulated. Also tabulated are the currents and current directions observed at 2200 GMT on Dec. 9 by the OSCR system at cells 490, 517 and 544. Cells 544 and 490 correspond closely to the starting and ending locations, respectively, of the CODE drifter. Cell 517 is intermediate between cells 544 and 490 (see Figure 6). From Table 4, we note that the AMP drifters generally measure a current on the order of 20 cm/s with a direction on the order of 245°. The CODE drifter gives a current of 11 cm/s with a direction of 252° and the OSCR system gives a current on the order of 8 cm/s with a direction on the order of 230°. The differences in the observed current magnitudes are a consequence of the different depth-averaging characteristics of the three measurement systems. For simplicity, we let $U(z_0)$ represent a unidirectional but depth varying current with the vertical coordinate z_0 increasing downward from the water surface. Then, for both the AMP and CODE drifters, the measured current U_m is given by

$$U_m = \left[\frac{1}{L}\int_0^L U^2(z_0)\,dz_0\right]^{1/2} \tag{11}$$

where L is the depth of penetration of the drifter. For a current which diminishes in magnitude with increasing depth, equation (11) provides that the AMP drifters would give, and as was found, a larger current than the CODE drifter since the L for the AMP drifters (3.5 cm) is

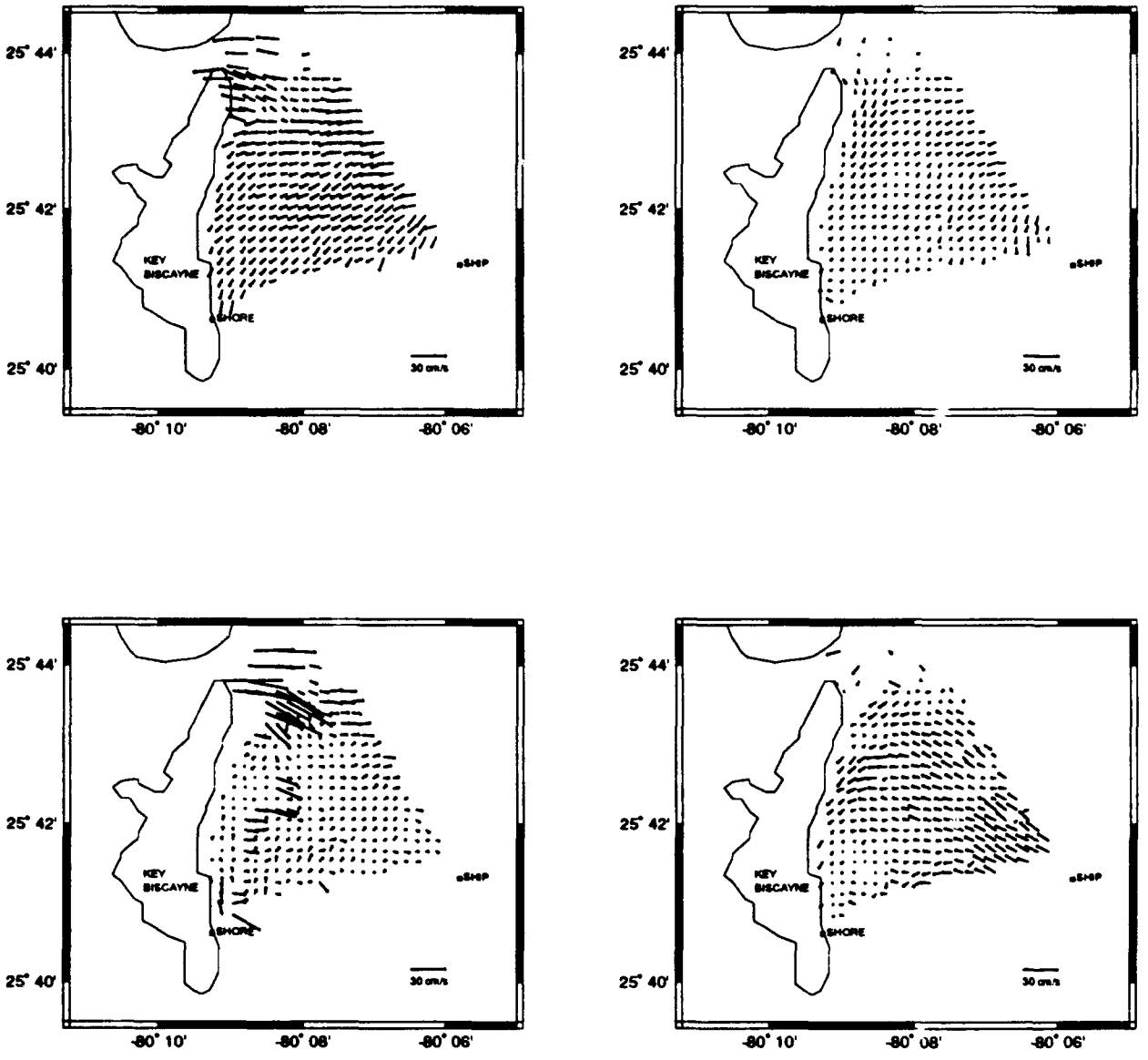

FIGURE 15. Surface current maps: (upper left) incoming tide at 2200 GMT on Dec. 9; (upper right) high tide near 2300 GMT on Dec. 9; (lower left) outgoing tide at 0200 GMT on Dec. 10; (lower right) low tide near 0500 GMT on Dec. 10.

TABLE 3. Drifter Deployment on Dec. 9 during OSCR Shipboard Experiment

Drifter	Start Time (GMT) End Time (GMT)	Start Latitude (N) End Latitude (N)	Start Longitude (W) End Longitude (W)
AMP #2	1856.5	25° 41.734'	80° 06.352'
	1925.0	25° 41.639'	80° 06.575'
AMP #3	1901.0	25° 41.824'	80° 06.522'
	1939.0	25° 41.736'	80° 06.809'
AMP #4	1918.5	25° 41.825'	80° 06.819'
	2030.0	25° 41.612'	80° 07.276'
AMP #5	1920.0	25° 41.871'	80° 07.034'
	2034.0	25° 41.622'	80° 07.517'
AMP #6	1925.0	25° 41.698'	80° 06.444'
	2000.0	25° 41.603'	80° 06.653'
CODE	1856.0	25° 41.720'	80° 06.307'
	2039.0	25° 41.599'	80° 06.710'

TABLE 4. Drifter/OSCR Currents and Current Directions

Source	Mean Current (cm/s)	Mean Direction (deg)
AMP #2	24	245
AMP #3	22	251
AMP #4	20	243
AMP #5	21	240
AMP #6	19	243
CODE	11	252
OSCR (Cell 490)†	7	223
OSCR (Cell 517)†	8	229
OSCR (Cell 544)†	8	231

† Data at 2200 GMT on Dec. 9

smaller than the L for the CODE drifter (1 m). For the OSCR system, the measured current is given by (Stewart and Joy, 1974)

$$U_m = \frac{4\pi}{\lambda} \int_0^{\infty} U(z_0)\, e^{\frac{-4\pi z_0}{\lambda}}\, dz_0 \qquad (12)$$

where, as previously, λ is the Bragg resonant wavelength (3 m for the OSCR VHF mode) and where we have assumed infinite water depth. Skop (1987) has extended equation (12) to water of finite depth but the differences between his expression and equation (12) are not substantive for the depths and wavelengths encountered during the OSCR shipboard experiment. It is difficult to compare equations (11) and (12) directly. However, for the CODE drifter and for the OSCR system, both equations essentially represent an average of the current over the upper meter of water. Hence, and as was found, the observed currents for the CODE drifter and the OSCR system should be comparable. The small deviations in the observed direction of the current between the OSCR system and the AMP and CODE drifters is most likely a consequence of a slow variation in the direction of the tidal flow during the period between the drifter deployment and the OSCR measurements. Overall, the three systems render a consistent picture of the incoming tidal flow between 1900 and 2200 GMT on Dec. 9.

Conclusions

The capability to deploy an OSCR site offshore to map nearshore coastal currents has been demonstrated. Provided that the motions of the support platform are moderately restrained and that the system is mounted so as to avoid superstructure effects, high quality vector current maps can be obtained. During our experiment, we have shown the validity of these maps through comparisons with shore based measurements, known tidal flows and drifter observations.

The capability to deploy an OSCR type system offshore leads to the potential for wide area, long term, real time monitoring of nearshore coastal currents. This potential would be useful in many coastal survey operations. The capability also leads to the potential for rapid change in the area of coverage via moving the locations of the support platforms. This potential would be useful in predicting the trajectories of nearshore spills of oil and other hazardous materials.

Acknowledgements

The authors gratefully acknowledge funding support by the Naval Research Laboratory (SSC) under grant N00014-93-1-G900. We also acknowledge our many useful conversations with Mr. Ken Ferer (NRL-SSC), Dr. Dennis Trizna (ONR) and Dr. Hans Graber (RSMAS) in guiding the scope and execution of this project. We thank Drs. John Brown and Gary Hitchcock and Mr. Lou Chemi, all from RSMAS, for making the drifter measurements and Mr. Jorge Martinez (RSMAS) for tending to the OSCR onshore site. Finally, we thank Mr. Buddy

Davidson (RSMAS) for his invaluable assistance in setting up and running both the OSCR shipboard site and the ship motion measurement system.

References

Barrick, D.E., 1972. First-order theory and analysis of MF/HF/VHF scatter from the sea. IEEE Trans. Antennas Propagat., AP-20, 2-10.
Brigham, E.O., 1974. The Fast Fourier Transform. Prentice-Hall, Englewood Cliffs, NJ.

Chemi, L., H.C. Graber, D.B. Ross and L.K. Shay, 1993. Fields of ocean surface currents during HIRES-I. RSMAS Technical Report 93-004.

Oppenheim, A.V., A.S. Willsky and I.T. Young, 1983. Signals and Systems. Prentice-Hall, Englewood Cliffs, NJ.

Prandle, D., 1987. The fine-structrue of nearshore tidal and residual circulations revealed by HF radar surface current measurements. J. Phys. Oceanogr., 17, 231-245.

Schott, F., A.S. Frisch, K. Leaman, G. Samuels and I.P. Fotiro, 1986. High-frequency Doppler radar measurements of the Florida Current in summer 1983. J. Geophys. Res., 90, 9006-9016.

Shay, L.K., D.B. Ross and H.C. Graber, 1992. Ocean surface current profiling using HF Radar. RSMAS Technical Report 92-004.

Skop, R.A., 1987. Approximate dispersion relation for wave-current interactions. J. Waterway, Port, Coastal, and Ocean Engrg., ASCE, 113, 187-195.

Stewart, R.H. and J.W. Joy, 1974. HF radio measurements of surface currents. Deep Sea Res., 21, 1039-1049.

REPORT DOCUMENTATION PAGE

Form Approved
OMB No 0704-0188

1. AGENCY USE ONLY (Leave blank)	2. REPORT DATE	3. REPORT TYPE AND DATES COVERED
	March 1994	

4. TITLE AND SUBTITLE

MEASUREMENTS OF COASTAL CURRENTS USING A SHIP BASED VHF RADAR SYSTEM

5. FUNDING NUMBERS

N00014-93-1-G900

6. AUTHOR(S)

Richard A. Skop, Duncan B. Ross, Nicholas J. Peters and Lila Chamberlain

7. PERFORMING ORGANIZATION NAME(S) AND ADDRESS(ES)

Division of Applied Marine Physics
Rosenstiel School of Marine & Atmospheric Science
University of Miami, 4600 Rickenbacker Causeway
Miami, FL 33149

8. PERFORMING ORGANIZATION REPORT NUMBER

RSMAS Technical Report 94-001

9. SPONSORING/MONITORING AGENCY NAME(S) AND ADDRESS(ES)

Naval Research Laboratory (SSC)
Code 7410
Stennis Space Center, MS 39529

Office of Naval Research
Remote Sensing Program
800 N. Quincy Street
Arlington, VA 22217

10. SPONSORING/MONITORING AGENCY REPORT NUMBER

11. SUPPLEMENTARY NOTES

12a. DISTRIBUTION/AVAILABILITY STATEMENT

Approved for public release. Distribution unlimited.

12b. DISTRIBUTION CODE

13. ABSTRACT (Maximum 200 words)

The University of Miami Ocean Surface Current Radar (OSCR) is a pulsed radar which utilizes a Yagi transmit antenna and a phased, line array receive antenna. In its VHF (50 MHz) mode of operation, the system has a range of 12 km and a resolution of 250 m. The Bragg resonant wavelength is 3 m. In December 1993, one of two OSCR VHF sites was configured aboard the 50 m research vessel COLUMBUS ISELIN, anchored in a four-point mooring 5 km from the second site on Key Biscayne, FL. A six channel accelerometer system was used to obtain ship motion measurements. The purpose of this experiment was an initial evaluation of using an OSCR type system to map nearshore coastal currents from a ship. Our results show that high quality vector current maps can be obtained provided that the motions of the support platform are moderately restrained and that the system is mounted so as to avoid superstructure effects. During our experiment, we have also shown the validity of these maps through comparisons with shore based measurements, known tidal flows and drifter observations.

The capability to deploy an OSCR type system offshore leads to the potential for wide area, long term, real time monitoring of nearshore coastal currents. This potential would be useful in many coastal survey operations. The capability also leads to the potential for rapid change in the area of coverage via moving the locations of the support platforms. This potential would be useful in predicting the trajectories of nearshore spills of oil and other hazardous materials.

14. SUBJECT TERMS

VHF Radar, Surface Currents, Coastal Currents, Radar Backscatter, Remote Sensing

15. NUMBER OF PAGES

28

16. PRICE CODE

17. SECURITY CLASSIFICATION OF REPORT	18. SECURITY CLASSIFICATION OF THIS PAGE	19. SECURITY CLASSIFICATION OF ABSTRACT	20. LIMITATION OF ABSTRACT
Unclassified	Unclassified	Unclassified	